Dyadic Green's Functions of a Laminar Plate

Alexandre Reinhardt, Vincent Laude, *Member, IEEE*, Abdelkrim Khelif, and Sylvain Ballandras

***Abstract*—We introduce the concept of dyadic Green's functions of a laminar plate. These functions generalize classical Green's functions. In addition to relating displacements and stresses at the surface of a medium, they relate these quantities at both the top and the bottom surfaces of a medium of finite thickness and infinite extent in the transverse directions. We describe here the calculation of these functions in the spectral domain and provide some academic examples demonstrating their interest.**

I. Introduction

Surface Green's functions, that relate displacements to stresses at the surface of a semi-infinite or multilayered substrate, are a powerful tool to study wave propagation. They are efficient in elastic surface wave analysis where they enable, for instance, the characterization of modes and the understanding of their behavior [1]–[3]. They are also used in the mixed finite element analysis/boundary element method (FEA/BEM) for fast and efficient calculation of the electromechanical behavior of structures radiating within a medium [4]–[6], or of guided elastic wave transducers made of inhomogeneous metal electrodes over or buried within stratified layers [7], [8]. In all of these models, surface Green's functions are calculated assuming either a semi-infinite or a finite laminar substrate with a stress-free bottom surface.

Some authors [9], [10] use Green's functions considering that the boundary delimiting a laminar layer is made of both its top and its bottom surfaces. As a consequence, their Green's functions tensors are twice the dimension of classical surface Green's functions. They also provide expressions for calculating them for an isotropic layer or for a composite system made of stacked homogeneous layers [11].

In the remainder of this paper, we assume the laminar plate is either a simple homogeneous plate or a multilayered medium of finite thickness. Layers in such a medium can be made of piezoelectric, insulating, or conducting materials, as well as of fluids, which can be considered ideal or can be viscous. They are assumed of infinite extent in the x_1 and x_3 directions following axis conventions defined in Fig. 1, and they present flat interfaces.

The aim of the Green's function of a laminar plate is to relate generalized displacements

Manuscript received February 12, 2004; accepted April 29, 2004.

The authors are with the Institut FEMTO-ST, LPMO department (formerly Laboratoire de Physique et Métrologie des Oscillateurs (LPMO)), associé à l'Université de Franche-Comté, 32 avenue de l'Observatoire, 25 044 Besançon Cedex, France (e-mail: alexandre.reinhardt@lpmo.edu).

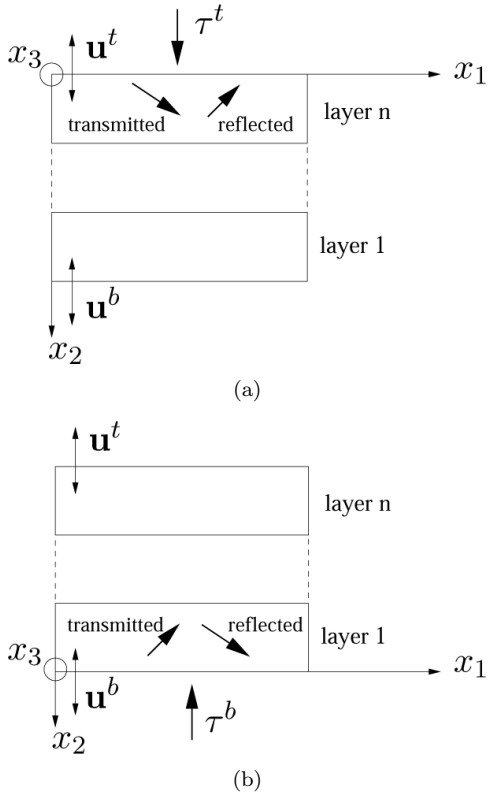

Fig. 1. Axes conventions and definitions of displacements and stress vectors for (a) the structure when applying stresses to the top surface, and (b) when applying stresses to the bottom surface.

$$\mathbf{u} = \begin{pmatrix} \mathbf{u}^t \\ \mathbf{u}^b \end{pmatrix} = \begin{pmatrix} u_1^t \\ u_2^t \\ u_3^t \\ \Phi^t \\ u_1^b \\ u_2^b \\ u_3^b \\ \Phi^b \end{pmatrix}, \tag{1}$$

composed of mechanical displacements u_i together with the electric potential Φ on both sides of a plate, to the generalized stresses

$$\tau = \begin{pmatrix} \tau^t \\ \tau^b \end{pmatrix} = \begin{pmatrix} T_{21}^t \\ T_{22}^t \\ T_{23}^t \\ D_2^t \\ T_{21}^b \\ T_{22}^b \\ T_{23}^b \\ D_2^b \end{pmatrix}, \tag{2}$$

composed of mechanical normal stresses T_{2i} together with the normal electric displacement D_2, applied on both sides on the boundaries of the structure, through

$$\mathbf{u} = G\tau, \tag{3}$$

and also by making use of the linearity of this definition to introduce notations that will be useful in the remaining of this paper

$$\begin{pmatrix} \mathbf{u}^t \\ \mathbf{u}^b \end{pmatrix} = \begin{pmatrix} G_{tt} & G_{tb} \\ G_{bt} & G_{bb} \end{pmatrix} \begin{pmatrix} \tau^t \\ \tau^b \end{pmatrix}. \tag{4}$$

Throughout this paper, we use the t and b superscripts for, respectively, the top and bottom sides of the plate. There are eight components for both displacements and stress vectors. Hence, the Green's function is an (8,8) matrix, or dyadic using Smith's denomination [12].

The calculation method is based on a modified Fahmy-Adler formulation, described in [13]. We recall shortly the method and provide definitions that will be necessary in the remaining of the paper. We then explain the calculation of the Green's dyadic and of its inverse. Finally, some academic examples of calculations are given to validate and illustrate this method.

II. Definitions

The model used to calculate the Green's functions of a laminar plate is based on a Fahmy-Adler formulation for waves in piezoelectric layers [14]. The vibration of a layer is described as the superposition of eight partial waves given by the solution of an eigenvalue problem that depends only on the material constants and on the slownesses s_1 and s_3 along x_1 and x_3 directions. The slownesses s_2 of partial waves are obtained as the eigenvalues, and thus provide the propagation constants of the corresponding partial waves, whereas polarizations are given by the corresponding eigenvectors. Finally, the electromechanical fields in layer number l are expressed as the state vector

$$\mathbf{h} = \begin{pmatrix} \mathbf{u} \\ \tau \end{pmatrix} = F_l \Delta_l(x_2) \mathbf{a}_l \exp j\omega(t - s_1 x_1 - s_3 x_3), \tag{5}$$

where F_l is the matrix containing the polarizations of partial waves, $\Delta_l(x_2) = \mathrm{diag}\,(\exp -2j\pi f s_{2i} x_2)$ is the diagonal matrix containing terms describing propagation along the x_2 direction, and $\mathbf{a}_l$ is the vector containing the amplitudes of partial waves. This formulation has been extended to fluids, ideal or with viscosity, and to perfectly conducting materials [15], [16]. For these materials, the number of partial waves can decrease because two partial waves of purely electrostatic polarizations (i.e., with polarizations along Φ and D_2 components only) are lost when considering perfectly conducting materials, and the partial waves of shear polarizations are also lost in nonviscous fluids. For these reasons, the F_l, $\Delta_l(x_2)$ matrices as well as the $\mathbf{a}_l$ and $\mathbf{h}$ vectors can shrink from dimension 8 to 6, 4, or even 2. For the sake of simplicity, we will describe the calculation for piezoelectrics (or also for viscous insulating fluids, which have mathematically the same behavior), and give only a few indications of the treatment of other types of materials when needed.

To be more stable at high frequencies the original formulation has also been modified by separating partial modes into two groups, using the following rules [13], [17]:

1. Transmitted partial waves have their acoustic power fleeing from the excitation surface, or are decaying exponentially when leaving the excitation surface. They correspond to homogeneous waves traveling away from the excitation surface (i.e., waves propagating from the top surface into the bulk for a semi-infinite medium) or to inhomogeneous waves guided at the vicinity of the surface.
2. Reflected partial waves have a Poynting vector directed towards the excitation surface, or are growing exponentially when leaving the excitation surface. They correspond to homogeneous waves incident on the excitation surface or to inhomogeneous waves guided at the vicinity of the excitation surface.

As a consequence of this definition, the partial waves selection is not the same in the two cases depicted in Fig. 1(a) and (b). Actually, the transmitted and reflected modes are exchanged between the two configurations.

From this partial waves selection rule, it is possible to introduce the reflection matrix $R_l(x_2)$ linking the reflected to transmitted partial waves in layer l [13], [15] as

$$\Delta_l^R(x_2)\mathbf{a}_l^R = R_l(x_2)\Delta_l^T(x_2)\mathbf{a}_l^T, \tag{6}$$

where the superscripts T and R indicate the restriction of matrices and vectors to transmitted and reflected partial waves, respectively.

III. Green's Functions Calculation

From (3), every component of the Green's matrix is defined as the ratio of a displacement over an applied stress, provided that all the other stress components are zero. Consequently, we first calculate the submatrices G_{tt} and G_{bt} by considering that stresses are applied at the top of the structure while the bottom surface is assumed stress-free. We then calculate G_{tb} and G_{bb} by considering stresses at the bottom of the structure while the top surface is stress-free.

A. Application of Stresses at the Top Surface

The stress-free bottom surface condition is expressed as

$$\Delta_1(x_b)\mathbf{a}_1 = F_1^{-1}\mathbf{h}(x_b) = F_1^{-1}\begin{pmatrix} I_4 \\ 0_4 \end{pmatrix}\mathbf{u}^b = \begin{pmatrix} A \\ B \end{pmatrix}\mathbf{u}^b, \tag{7}$$

where I_4 is the identity matrix of dimensions $(4,4)$, 0_4 is the null matrix of the same dimensions, and $\mathbf{u}^b$ is the

bottom displacements vector, not yet known. On the other hand, from the definition of reflection matrices, we also have

$$\Delta_1(x_b)\mathbf{a}_1 = \begin{pmatrix} I_4 \\ R_1(x_b) \end{pmatrix} \Delta_1^T(x_b)\mathbf{a}_1^T. \tag{8}$$

Equating these two expressions, the reflection matrix can be determined without the need to know explicitly the values of the bottom displacements, according to

$$R_1(x_b) = BA^{-1}. \tag{9}$$

The calculation for materials of a type other than piezoelectric was described in [15]; it is symbolically the same provided that the dimensions of the matrices are modified.

Once the reflection matrix at the bottom of the first layer is known, it is transferred to the top of this layer using the relation between reflection matrices at two points, x_2 and x_2', within the same layer l, [15]

$$R_l(x_2') = \Delta_l^R(x_2' - x_2)R_l(x_2)\Delta_l^T(x_2 - x_2'). \tag{10}$$

Partial wave conversion at the interface between two layers, indexed respectively l and $l+1$, is determined by stating that the components of the state vector are continuous across the interface. This leads to

$$\Delta_{l+1}(x_l)\mathbf{a}_{l+1} = \begin{pmatrix} C \\ D \end{pmatrix} \Delta_l^T(x_l)\mathbf{a}_l^T, \tag{11}$$

where x_l is the coordinate of the interface along x_2, and

$$\begin{pmatrix} C \\ D \end{pmatrix} = F_{l+1}^{-1}F_l \begin{pmatrix} I_4 \\ R_l(x_l) \end{pmatrix} \tag{12}$$

when the interface between two piezoelectric layers is considered. Since, in the general case, the size of matrices for layers l and $l+1$ may not be the same, it is necessary to make some hypotheses about the mechanical or electric behavior of materials at the interface. This involves considering a zero electric potential for conducting layers and making shear displacements vanish within nonviscous fluids. This leads to writing (11) in a symbolically analogous way, although the definitions of the C and D matrices are totally modified. Expressions for these matrices are provided in [15] as well as the exact hypotheses made to solve the partial wave conversion problem. Finally, the reflexion matrix is obtained as

$$R_{l+1}(x_l) = DC^{-1}. \tag{13}$$

Then, the reflection matrix is once again transferred to the top of the $(l+1)$-th layer using (10), and partial waves are converted to the next layer, and so on recursively until the top surface of the plate is reached.

At this step, the stress-free boundary condition applied to the bottom of the structure is transferred to the surface where the excitation stress is applied. We then write the definition of the state vector at the top surface as

$$\mathbf{h}(x_t) = \begin{pmatrix} \mathbf{u}^t \\ \tau^t \end{pmatrix} = \begin{pmatrix} E \\ F \end{pmatrix} \Delta_n^T(x_t)\mathbf{a}_n^T, \tag{14}$$

where n is the index of the topmost layer and

$$\begin{pmatrix} E \\ F \end{pmatrix} = F_n \begin{pmatrix} I_4 \\ R_n(x_t) \end{pmatrix} \tag{15}$$

in the case of a piezoelectric layer, and where x_t is the coordinate along the x_2 direction of the top surface of the structure. For other types of materials, the expression remains the same but the dimension of matrices is changed.

Selecting the last four lines of (14) yields the amplitudes of the transmitted partial waves under the excitation surface as a function of the applied stress as

$$\mathbf{a}_n^T = \Delta_n^{T-1}(x_t)F^{-1}\tau^t. \tag{16}$$

Top displacements are then given by the remaining part of (14),

$$\mathbf{u}^t = E\Delta_n^T(x_t)\mathbf{a}_n^T, \tag{17}$$

and thus submatrix G_{tt} can be determined. It is interesting to note that when inserting (16) into (17), the formula used for classical surface Green's functions [13], [15] is retrieved,

$$G_{tt} = EF^{-1}, \tag{18}$$

which shows that the approach described here is an extension of the usual one.

Considering again the conversion of partial waves at the interface between two layers, expressed by (11), one obtains

$$\mathbf{a}_l^T = \Delta_l^T(x_l)^{-1}C^{-1}\Delta_{l+1}^T(x_l)\mathbf{a}_{l+1}^T. \tag{19}$$

This relation shows that knowing the amplitudes of transmitted partial waves within a layer, it is possible to determine transmitted partial waves in the layer immediately underneath. Thus, by applying this formula recursively, it is possible to transfer the $\mathbf{a}^T$ vector from the topmost layer to the bottommost one. It is interesting to note that all matrices involved in this expression have already been calculated, so that this step does not represent a huge calculation overhead. Then, from (7) the bottom displacements are known as

$$\mathbf{u}^b = A^{-1}\Delta_1^T(x_b)\mathbf{a}_1^T, \tag{20}$$

where x_b is the coordinate along the x_2 direction of the bottom interface of the structure. The knowledge of the bottom displacements and of the top stress excitation enables the determination of submatrix G_{bt}.

B. Application of Stresses at the Bottom Surface

To calculate the second half of the Green's functions matrix, it is necessary to consider stresses applied at the bottom of the structure while the top surface remains stress-free. To do this, we apply the same scheme as when imposing stresses at the top surface.

We start by writing the definition of the reflexion matrix on the stress-free surface,

$$\Delta_n(x_t)\mathbf{a}_n = \begin{pmatrix} I_4 \\ R_n(x_t) \end{pmatrix} \Delta_n^T(x_t)\mathbf{a}_n^T = \begin{pmatrix} A \\ B \end{pmatrix} \mathbf{u}^t, \tag{21}$$

where

$$\begin{pmatrix} A \\ B \end{pmatrix} = F_n^{-1} \begin{pmatrix} I_4 \\ 0_4 \end{pmatrix}. \tag{22}$$

These equations are obviously similar to (8) and (7), with the only difference being that the considered layer is n and not 1. Thus, (9) remains valid in our case provided that the index of the layer is changed. As the definition of reflection matrices remains unchanged, (10) also remains valid. However, this time, reflection matrices are transferred from the top to the bottom of the layers, so that the sign of the argument of the Δ matrices, which physically corresponds to the algebraic propagation length of waves, becomes negative; it was positive when application of stresses at the top surface were considered. This is caused by the fact that the partial waves selection rule inverts the classification of partial modes in the two configurations and thus, for propagating waves, their propagation directions or, for inhomogeneous waves, the directions in which they are decreasing.

When considering the conversion of partial waves between two layers, this time we know the reflection matrix at the bottom of the upper layer, say, $l+1$, and our goal is to calculate the reflection matrix in the layer underneath, say, l. Thus, the continuity of electromechanical fields at the interface is expressed as

$$\Delta_l(x_{l+1})\mathbf{a}_l = \begin{pmatrix} C \\ D \end{pmatrix} \Delta_{l+1}^T(x_{l+1})\mathbf{a}_{l+1}^T, \tag{23}$$

where x_{l+1} is the coordinate of the interface along x_2, and

$$\begin{pmatrix} C \\ D \end{pmatrix} = F_l^{-1} F_{l+1} \begin{pmatrix} I_4 \\ R_{l+1}(x_{l+1}) \end{pmatrix} \tag{24}$$

when two piezoelectric layers are considered. Once again, these relations are formally equivalent to (11) and (12) although indices l and $l+1$ need to be exchanged because of the inversion of the order in which layers are considered when the reflection matrices are calculated. So, in the same way as we have transferred the bottom stress-free surface boundary condition to the top surface in Section III-A, we are able here to transfer the top stress-free surface boundary condition to the bottom surface of the structure.

Finally, let us consider the application of stresses at the bottom of the multilayer

$$\mathbf{h}(x_b) = \begin{pmatrix} \mathbf{u}^b \\ \tau^b \end{pmatrix} = \begin{pmatrix} E \\ F \end{pmatrix} \Delta_1^T(x_b)\mathbf{a}_1^T, \tag{25}$$

where

$$\begin{pmatrix} E \\ F \end{pmatrix} = F_1 \begin{pmatrix} I_4 \\ R_1(x_b) \end{pmatrix} \tag{26}$$

for a piezoelectric layer. These relations are also formally equivalent to those written when stresses at the top of the structure are applied.

So, instead of rewriting all the equations, we rather use the same algorithm for the excitation both at the top and at the bottom of the multilayer, with the following differences when exciting at the bottom:

1. The partial modes selection rule needs to be inverted according to the general rule expressed earlier.
2. The algorithm processes the layers in an upwards way when exciting at the top of the structure, whereas it operates downwards when exciting at the bottom. To reuse exactly the same equations, it is convenient to reverse the order of the layers. This causes also the t and b subscripts to be exchanged.
3. The transfer of reflection matrices needs to be performed only from one side of a layer to the other side. So, only its thickness is to be considered. Thus, when exciting at the bottom, it is convenient to use the same transfer equations, but with "negative" thicknesses.

Albeit these three points, all of the algorithm applied in the Section III-A remains totally valid, and hence the calculations of G_{tb} and G_{bb} is respectively the same as those of G_{bt} and G_{tt}.

IV. Calculation of the Inverse of the Green's Functions

The inverse of the dyadic Green's function is defined as

$$\tau = G^{-1}\mathbf{u}, \tag{27}$$

and can be divided into submatrices

$$G^{-1} = \begin{pmatrix} \mathcal{G}_{tt}^{-1} & \mathcal{G}_{tb}^{-1} \\ \mathcal{G}_{bt}^{-1} & \mathcal{G}_{bb}^{-1} \end{pmatrix}. \tag{28}$$

Simply inverting the 8×8 matrix can lead to numerical instabilities, as we have experienced, because some components can exhibit singularities, especially the electrostatic ones (i.e., G_{44} and G_{88}) which have a logarithmic behavior when surface slownesses are close to zero. Thus, it is necessary to calculate separately the inverse of the Green's function matrix. The algorithm used is very similar to the one described in Section III.

First, the calculation of the reflection matrix is initialized at the bottom of the structure. Instead of being concerned with a stress-free surface, the definition of the inverse of the Green's function matrix in (27) implies that each component in the matrix is the ratio of a generated stress component over an imposed displacement, while the other displacements are forced to zero. Thus, when a displacement is imposed on the top surface, the bottom surface needs to be considered clamped. This condition is written in a form similar to (7) as

$$\Delta_1(x_b)\mathbf{a}_1 = F_1^{-1} \begin{pmatrix} 0_4 \\ I_4 \end{pmatrix} \tau^b = \begin{pmatrix} A' \\ B' \end{pmatrix} \tau^b. \tag{29}$$

This leads to the expression of the reflection matrix at the bottom of the structure

$$R_1(x_b) = B' A'^{-1}. \tag{30}$$

Once the calculation of the reflection matrix is initiated, its transfer to the top surface is performed in the same way as for the standard algorithm.

At the top surface, displacements rather than stresses are imposed, but (14) remains valid. We can consequently use its first four lines to obtain the amplitudes of partial transmitted modes within the first layer

$$\mathbf{a}_n^T = \Delta_n^T(x_t)^{-1} E'^{-1} \mathbf{u}^t. \tag{31}$$

Using the last four lines of (10) we get the stress components at the top surface

$$\tau^t = F' \Delta_n^T(x_t) \mathbf{a}_n^T, \tag{32}$$

and thus the components of the submatrix $\mathcal{G}_{tt}^{-1}$. As for the calculation of the direct Green's function, inserting (31) into (32) provides the relation

$$\tau^t = F' E'^{-1} \mathbf{u}^t, \tag{33}$$

which corresponds to the expression used for calculating the inverse of the classical Green's functions [13]. But unlike the calculation of direct Green's functions, this is only a symbolic analogy. In fact, we previously calculated the classical Green's functions with a bottom stress-free surface condition, whereas here it is obtained for a bottom clamped surface. So, in this case, the current approach is also an extension of the classical concept.

The next step in the algorithm is to calculate the amplitudes of transmitted partial waves in all other layers, as explained in the Section III-A subsection. Then at last, the bottom stress vector is obtained using the four first lines of (29) as

$$\tau^b = A'^{-1} \Delta_1^T(x_b) \mathbf{a}_1^T. \tag{34}$$

This provides the components of $\mathcal{G}_{bt}^{-1}$.

The remaining part of the matrix is calculated after an inversion of the structure, using the rules described in subsection Section III-B, and a new run of the algorithm we have just described.

V. Numerical Examples

Now that we have shown how to calculate the dyadic Green's functions of a laminar plate, we will provide some academic examples.

A. Thickness Extensional Response of a Plate

We consider in this example a simple plate on which harmonic traction forces $F = F_0 \exp j\omega t$ are applied at each side, as shown in Fig. 2. This problem can be solved analytically by considering that solely a longitudinal wave travels vertically in the plate. As demonstrated in the appendix, normal top displacements are given by

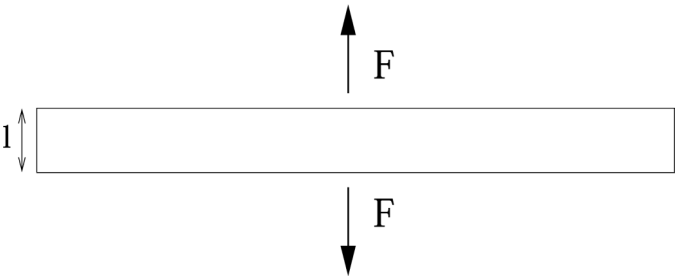

Fig. 2. A simple plate on which traction forces are applied.

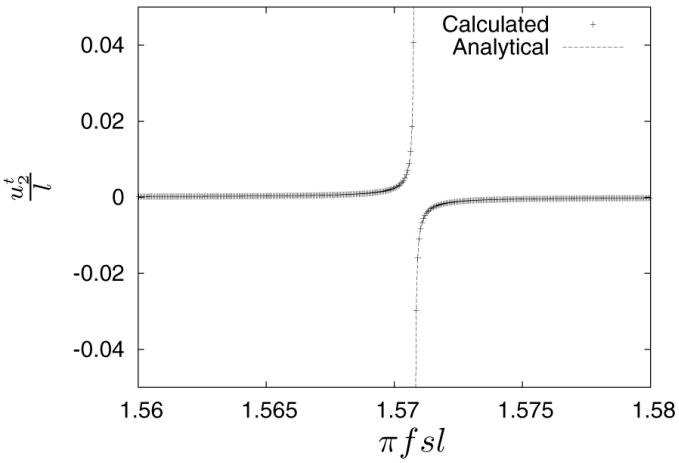

Fig. 3. Comparison between analytical expression and calculated Green's functions for the thickness extension of a simple plate.

$$u_2^t = \frac{F_0}{2\pi f s c} \tan(\pi f s l \exp j\omega t), \tag{35}$$

where s is the slowness of the longitudinal wave within the material, c is its elastic modulus in the vertical direction, and l is the thickness of the plate. In Fig. 3, we compare both the analytical formula and the displacements given by the use of the Green's function $u_2^t = (G_{22}+G_{26})F_0 \exp j\omega t$. The two approaches agree very well, and provide an analytical validation for the model.

B. Acoustic Coupling Between Two Resonators in a Coupled Resonator Filter

The second example consists of the study of the coupling between resonators in coupled resonator filters (CRF). Such devices, introduced by Lakin *et al.* [18], are made of two or more resonators piled up vertically, separated by a few quarter-wavelength layers, so that vibrations generated by one of the resonators are partially transmitted to the other, as depicted in Fig. 4. A set of coupled resonators is thus created and, provided their resonances are close enough, a filter transmission function is achieved. The coupling of the resonators is directly related to the isolation layers inserted between them [19]. These layers act as a Bragg mirror that causes acoustic power to be

Fig. 4. Basic structure for a coupled resonator filter.

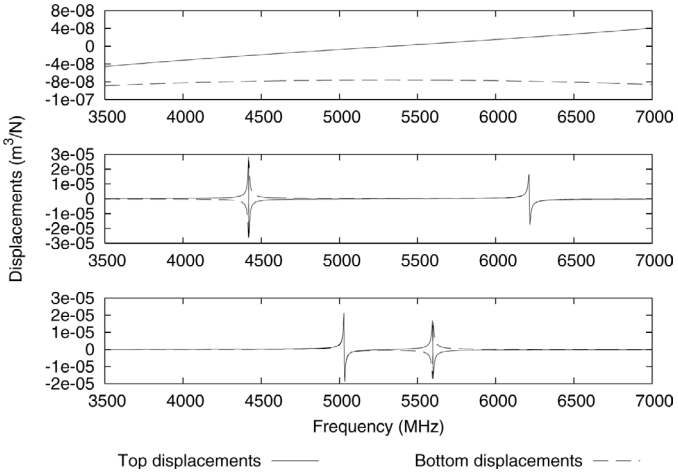

Fig. 5. G_{22} and G_{62} for various isolation layers configurations. From top to bottom: a single silica quarter-wavelength layer, silica/AlN/silica, and silica/AlN/silica/AlN/silica. Each layer is quarter-wavelength thick at the center frequency of 5.25 GHz.

trapped within the resonators. Thus the coupling is performed through evanescent fields.

In this example, we focus only on the transmission properties of the coupling layers. In Fig. 5 we show the calculated displacements at the top and bottom surfaces of the isolation layers when a harmonic stress is applied at the top surface. For a single layer, the displacements are quite regular, but one can note that at the center frequency the transmitted and reflected longitudinal waves interfere destructively at the top of the quarter-wavelength layer, and thus the displacements are kept near zero at the top surface. When more layers are involved, the spectrum becomes more complicated, due to partial reflections inside the structure. In particular, two thickness modes appear. They are used to provide the filter function, although the mass loading of the resonators shifts their resonance frequencies.

We define a displacement ratio as

$$\rho_u = \left| \frac{u_2^b}{u_2^t} \right| = \left| \frac{G_{22}}{G_{26}} \right|, \tag{36}$$

which is reported in Fig. 6. The isolation layers exhibit a peak in the displacement ratio at the center frequency, which favors the coupling between the two resonators in a CRF. However, the transmission decreases with the number of layers, which is consistent with the fact that for a Bragg mirror the reflection coefficient increases with the number of layers. It is also interesting to note that the

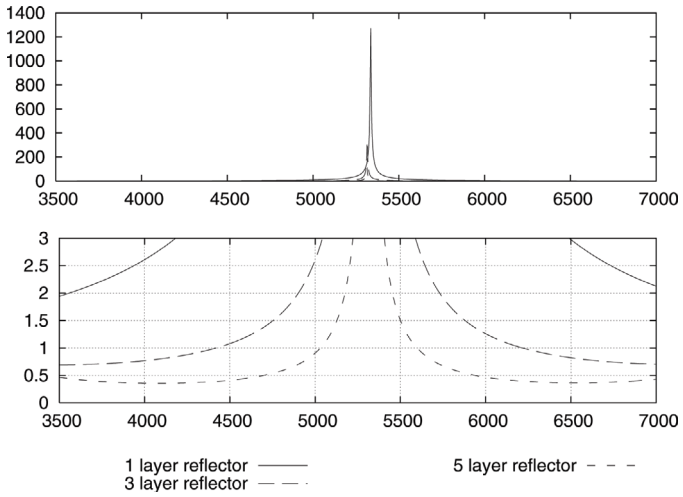

Fig. 6. Displacement ratio of bottom normal displacements over top normal displacements versus frequency for the same isolation layers as in the previous figure. Top: full scale spectrum; bottom: zoom of the spectrum near unity value.

two mechanical resonances seen earlier are located at frequencies where the displacement ratio is equal to 1. This corresponds to the transition between the regions where acoustic power is transmitted (corresponding to the filter passband in a CRF) and the one where acoustic power is reflected (corresponding to the rejection band in filters).

VI. Conclusions

We have introduced the concept of dyadic Green's functions of a laminar plate, which relate displacements at the top and bottom surfaces to the stresses applied at these surfaces for a medium of finite thickness. We have described an algorithm to calculate these functions and their inverse for multilayered plates of infinite extent in the horizontal directions, consisting of piezoelectric, dielectric, and conducting materials, as well as fluids, viscous or not. Some examples have then been given to validate the model and demonstrate some applications it can be useful for.

The main foreseen application of this tool is its inclusion within an FEA/BIM. It should now become possible to introduce boundary elements within complicated meshes, and not only at their extremities. Although the dimension of the matrices to manipulate is increased, compared to classical Green's functions, the gain in calculation complexity should be noticeable.

Appendix A
Analytic Calculation of the Thickness-Extensional Response of a Single Plate

Let us consider the plate depicted in Fig. 2 in which a longitudinal wave propagates vertically with slowness $s = \sqrt{\frac{\rho}{c}}$, where ρ is the mass density of the material, and c its elastic modulus. Thus, the expression of vertical displacements is

$$u_2 = A \exp j\omega(t - sx_2) + B \exp j\omega(t + sx_2). \tag{37}$$

From Hooke's law,

$$T_{ij} = c_{ijkl} S_{kl} \tag{38}$$

where c_{ijkl} are the components of the elastic tensor, and S_{kl} the components of the strain tensor. From the definition of the strain components

$$S_{kl} = \frac{1}{2}\left(\frac{\partial u_k}{\partial x_l} + \frac{\partial u_l}{\partial x_k}\right) \tag{39}$$

and the symmetry properties of the elastic tensor, one gets

$$T_{22} = c\frac{\partial u_2}{\partial x_2}. \tag{40}$$

This equation remains valid for piezoelectric materials if the stiffening of elastic constants due to piezoelectricity is applied. Inserting (37) into this expression provides the expression of stresses associated with the longitudinal wave:

$$T_{22} = -j\omega s(A \exp(j\omega(t - sx_2)) - B \exp(j\omega(t + sx_2))). \tag{41}$$

The boundary conditions are that the stresses are imposed on both sides of the plate, or

$$T_{22}\left(x_2 = \frac{l}{2}\right) = F_0 \exp j\omega t, \tag{42}$$

$$T_{22}\left(x_2 = -\frac{l}{2}\right) = -F_0 \exp j\omega t. \tag{43}$$

From the expression of stresses, the following equations are obtained

$$(A - B)\cos\frac{\omega s l}{2} = 0, \tag{44}$$

$$2\omega c s (A + B)\sin\frac{\omega s l}{2} = 2F_0. \tag{45}$$

Thus,

$$A = B = \frac{F_0}{2\omega c s \sin\frac{\omega s l}{2}}, \tag{46}$$

and the expression for displacements of the top surface become

$$u_2^t = \frac{F_0}{\omega c s}\tan\left(\frac{\omega s l}{2}\right)\exp j\omega t. \tag{47}$$

Acknowledgment

The authors are grateful to Sarah Benchabane for enlightening discussions.

References

[1] V. P. Plessky and T. Thorvaldsson, "Rayleigh waves and leaky SAW in periodic systems of electrodes: Periodic Green's function analysis," in *Proc. IEEE Ultrason. Symp.*, 1992, pp. 461–464.

[2] R. Peach, "On the existence of surface acoustic waves on piezoelectric substrates," *IEEE Trans. Ultrason., Ferroelect., Freq. Contr.*, vol. 48, no. 5, Sep. 2001.

[3] D. A. Powell, K. Kalantar-Zadeh, and W. Wlodarski, "Comprehensive analysis of SAW sensor performance in liquid media by Green's function method," in *Proc. IEEE Ultrason. Symp.*, Oct. 2003, pp. 146–149.

[4] H. P. Reichinger and A. R. Baghai-Wadji, "Dynamic 2D analysis of SAW-devices including massloading," in *Proc. IEEE Ultrason. Symp.*, 1992, pp. 7–10.

[5] P. Ventura, J. M. Hodé, M. Solal, J. Desbois, and J Ribbe, "Numerical methods for SAW propagation characterization," in *Proc. IEEE Ultrason. Symp.*, 1998, pp. 175–186.

[6] P. Ventura, J. M. Hodé, J. Desbois, and M. Solal, "Combined FEM and Green's function analysis of periodic SAW structure, application to the calculation of reflection and scattering parameters," *IEEE Trans. Ultrason., Ferroelect., Freq. Contr.*, vol. 48, no. 5, pp. 1259–1273, Sep. 2001.

[7] S. Camou, S Ballandras, and T. Pastureaud, "A mixed FEM/BEM model to characterize surface waves on multilayer substrate," in *Proc. IEEE Ultrason. Symp.*, 1999, pp. 143–146.

[8] S. Ballandras, V. Laude, T. Pastureaud, M. Wilm, W. Daniau, A. Reinhardt, W. Steichen, and R. Lardat, "A FEA/BEM approach to simulate complex electrode structures devoted to guided elastic wave periodic transducers," in *2003 World Congr. Ultrasound Proc.*, Paris, Sep. 2003, pp. 927–930.

[9] E. H. El Boudouti, B. Djafari-Rouhani, and A. Akjouj, "Resonant guided elastic waves in an adsorbed bilayer: Theoretical analysis of the density of states," *Phys. Rev. B*, vol. 55, no. 7, pp. 4442–4448, Feb. 1997.

[10] D. Bria and B. Djafari-Rouhani, "Omnidirectional elastic band gap in finite lamellar structures," *Phys. Rev. E*, vol. 66, 2002.

[11] P. A. Deymier, J. O. Vasseur, A. Khelif, B. Djafari-Rouhani, L. Dobrzynski, and S. Raghavan, "Streaming and removal forces due to second-order sound field during megasonic cleaning of silicon wafers," *J. Appl. Phys.*, vol. 88, no. 11, pp. 6821–6835, Dec. 2000.

[12] P. M. Smith, "Dyadic Green's functions for multi-layer SAW substrates," *IEEE Trans. Ultrason., Ferroelect., Freq. Contr.*, vol. 48, no. 1, pp. 171–179, 2001.

[13] T. Pastureaud, V. Laude, and S. Ballandras, "Stable scattering-matrix method for surface acoustic waves in piezoelectric multilayers," *Appl. Phys. Lett.*, vol. 80, no. 14, pp. 2544–2546, Apr. 2002.

[14] E. L. Adler, "Matrix methods applied to acoustic waves in multilayers," *IEEE Trans. Ultrason., Ferroelect., Freq. Contr.*, vol. 37, no. 6, pp. 485–490, Nov. 1990.

[15] A. Reinhardt, T. Pastureaud, S. Ballandras, and V. Laude, "Scattering matrix method for modeling acoustic waves in piezoelectric, fluid, and metallic multilayers," *J. Appl. Phys.*, vol. 94, no. 10, pp. 6923–6931, Nov. 2003.

[16] S. Ballandras, A. Reinhardt, A. Khelif, M. Wilm, V. Laude, W. Daniau, V. Blondeau-Patissier, and W. Boireau, "Theoretical analysis of damping effects of SAW at solid/fluid interfaces," in *2003 Joint EFTF/IFCS Conf. Proc.*, Tampa, 2003, pp. 907–910.

[17] E. L. Tan, "A robust formulation of SAW Green's functions for arbitrarily thick multilayers at high frequencies," *IEEE Trans. Ultrason., Ferroelect., Freq. Contr.*, vol. 49, no. 7, pp. 929–936, Jul. 2002.

[18] K. M. Lakin, J. Belsick, J. F. McDonald, and K. T. McCarron, "High performance stacked crystal filters for GPS and wide bandwidth applications," in *Proc. IEEE Ultrason. Symp.*, 2001, pp. 833–838.

[19] A. Reinhardt, V. Laude, R. Lanz, P. Muralt, M. Solal, S. Ballandras, and W. Steichen, "Design of coupled resonator filters using admittance and scattering matrices," in *Proc. IEEE Ultrason. Symp.*, Honolulu, Oct. 2003.

Alexandre Reinhardt was born in 1977 in Pavillons-sous-Bois, France. He received an Engineering Diploma in 2001 from the Ecole Centrale de Lille, in Villeneuve d'Ascq, France, and a DEA in Electronics and Telecommunications, Ultrasonics from the Université de Valenciennes et du Hainault Cambresis, in Valenciennes, France, the same year. Then he joined the Laboratoire de Physique et Métrologie des Oscillateurs (LPMO) in Besançon, France, as a Ph.D. student, sponsored by Temex Microelectronics. He is working in the field of thin film bulk acoustic wave resonators (FBAR) and is especially interested in the modeling and the design of high-frequency wide bandwidth filters.

Vincent Laude (M'00) was born in Bourg-la-Reine, France, in 1968. He received an Engineering Diploma in 1990 from the Ecole Supérieure d'Optique, and a Ph.D. in Physics in 1994 from Paris XI University, both in Orsay, France. He received his Habilitation à Diriger des Recherches from the Université de Franche-Comté in 2002.

From 1995 to 1999, he was a researcher at Thomson-CSF Corporate Research Laboratory (now Thales TRT) in Orsay, France, where he worked on various aspects of optical signal processing, wavefront sensing, and ultrashort laser pulses. In 2000, he joined Thomson-CSF Microsonics in Sophia-Antipolis, France, to work on surface acoustic wave propagation. At the end of the same year, he joined the Laboratoire de Physique et Métrologie des Oscillateurs, Centre National de la Recherche Scientifique, in Besançon, France. He is currently interested in the propagation of surface, interface, and guided acoustic waves, their interaction with microstructures, phononic band gap materials, and acousto-optics.

Vincent Laude is a member of IEEE/UFFC.

Abdelkrim Khelif was born in 1971 in Bouira, Algeria. He received the DEA degree and the Ph.D. degree in Materials Science from the Université de Lille I. His thesis dissertation was dedicated to the theory of vibrations of and acoustic scattering by supported wires on a surface.

In 2000, he joined the Laboratoire de Physique des Solides of the University of Namur, Belgium, as a post-doctoral researcher. In 2002, he joined the Laboratoire de Physique et Métrologie des Oscillateurs, Centre National de la Recherche Scientifique in Besançon, France. He is currently interested in the propagation of acoustic waves in elastic band gap materials.

Sylvain Ballandras was born in 1965 in Strasbourg, France. He received the DEA in Acousto-Opto-Electronique et Vibrations and the Ph.D. degree in Science pour l'Ingénieur from the Université de Franche-Comté, Besançon, France.

He joined the Laboratoire de Physique et Métrologie des Oscillateurs (LPMO), Besançon, France, as a staff member in 1991. He has been working in the fields of SAW sensitivity to physical perturbations and in microtechnologies, such as LIGA and stereolithography. He received the Habilitation à Diriger des Recherches degree from the Université de Franche-Comté, in Besançon, France, in 1997. He joined Thomson Microsonics in Sophia Antipolis, France, for one year as a research engineer. He went back to the LPMO in 1998. Since 1999, he has been heading the Acoustics and Microsonics research group at the LPMO. His current interests are in the application of SAW devices (sensors) in the development of numerical models and new technologies for ultrasound transducers devoted to acoustic imaging and nondestructive control.